Electronic Supplementary Material (ESI) for Journal of Materials Chemistry A.

Supporting Information

Deep Insight of Ionic Transport in Polyampholyte Gel Polymer Electrolyte towards High Performance Solid Supercapacitor

Dong Li, Zhen Xu, Xingxiang Ji, Libin Liu*, Guangjie Gai, Jianbo Yang, Jijun Wang

Institute of Advanced Energy Materials and Chemistry, School of Chemistry and Pharmaceutical Engineering, State Key Laboratory of Biobased Material and Green Papermaking, Qilu University of Technology (Shandong Academy of Sciences), Jinan 250353, China,

Corresponding author. E-mail: lbliu@qlu.edu.cn (Libin Liu)

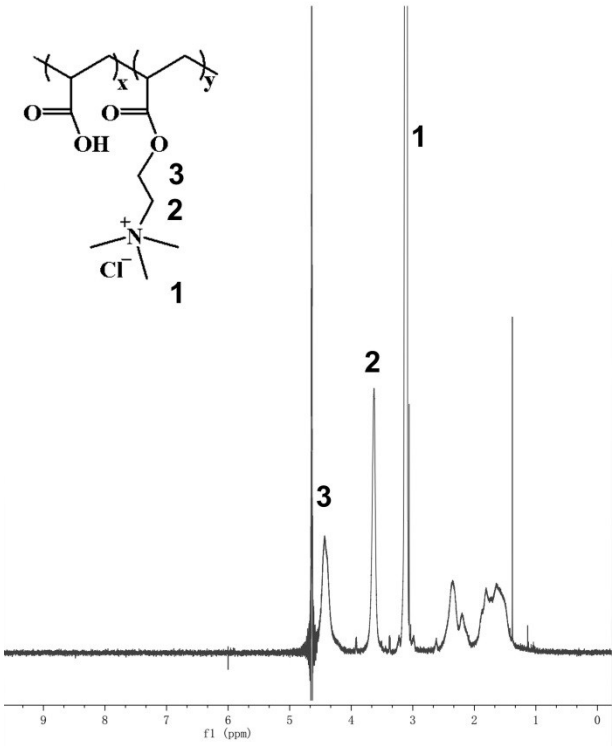

Figure S1. HNMR spectra of P(AA-DAC).

As shown in Figure S1, the $N^{+}(CH3)_3$ proton peaks of DAC were observed at 3.1 ppm. The –N-CH_2- proton peaks were located at 3.6 ppm. The –COO-CH_2- proton peaks were observed at 4.4 ppm. In the GPC measurement, for all the P(AA-DAC) samples, the weight average molecular weight varied between 4.29×10^4 and 4.71×10^4 g/mol and the polydispersity was in the range of 1.41~1.95.

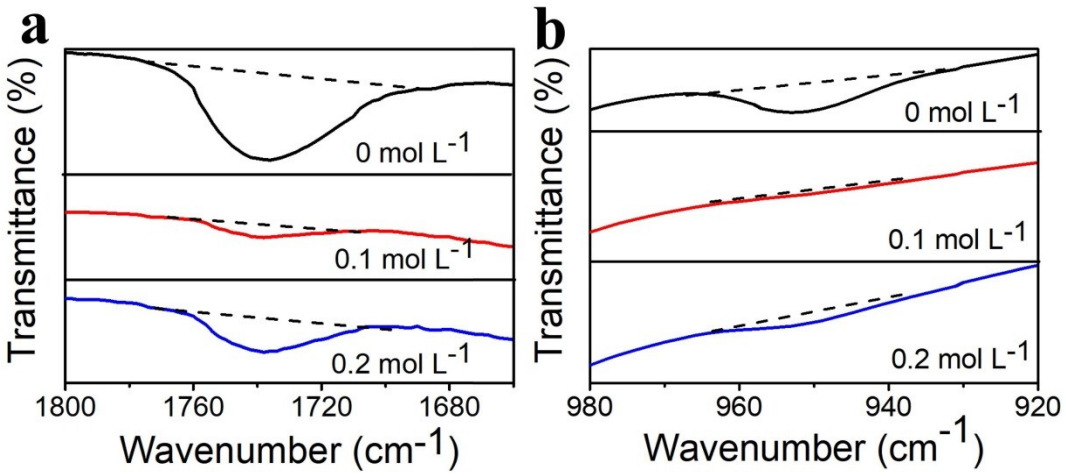

Figure S2. FTIR spectra of C=O group and $N^{+}(CH_3)_3$ group in P(AA_1-DAC_1) electrolyte with changes of LiCl content.

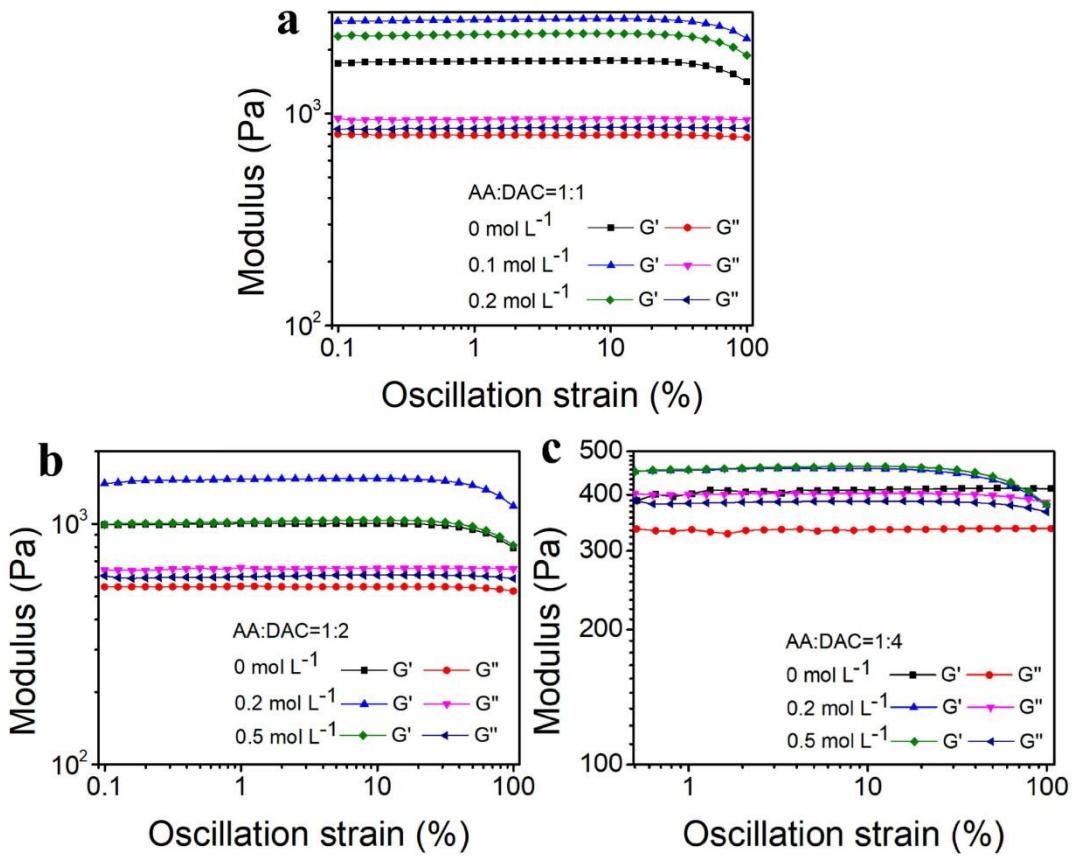

Figure S3. Storage (G') and loss (G'') modulus of of P(AA_1-DAC_1) (a), P(AA_1-DAC_2) (b) and P(AA_1-DAC_4) (c) electrolyte.

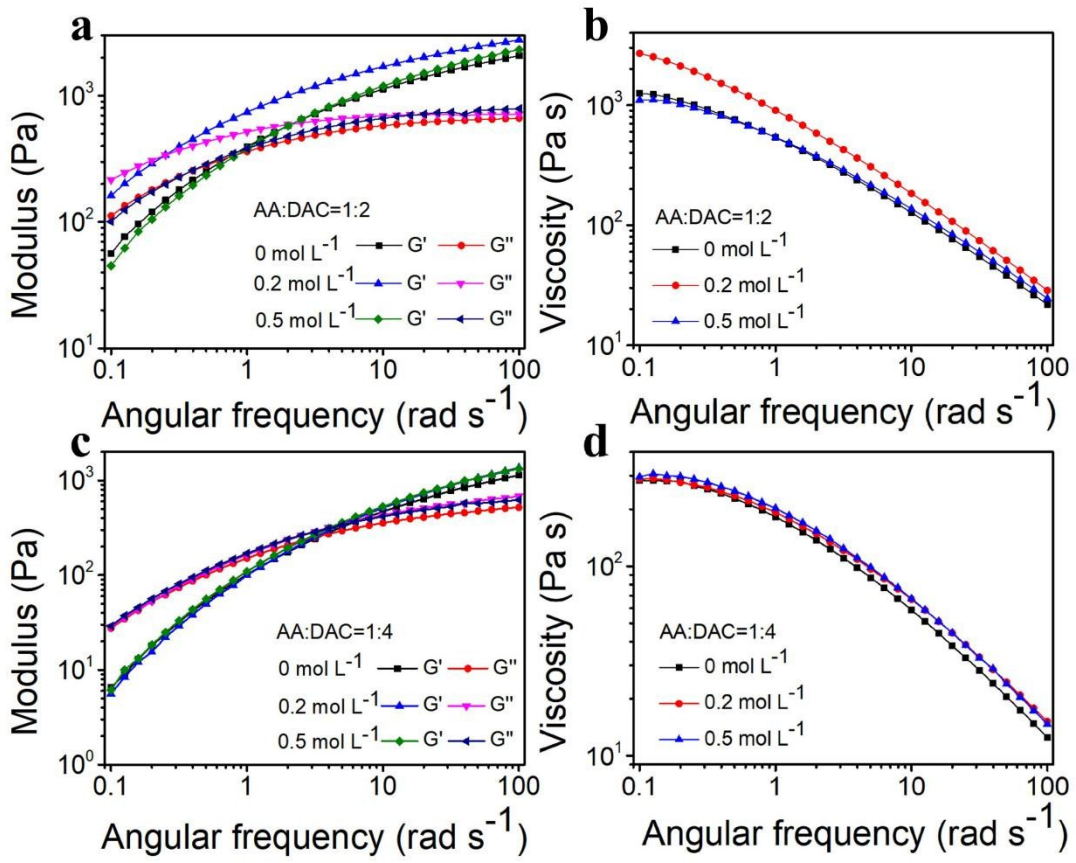

Figure S4. Storage (G') and loss (G'') modulus (a, c) and viscosity (b, d) of P(AA_1-DAC_2) (a, b) and P(AA_1-DAC_4) (c, d)electrolyte.

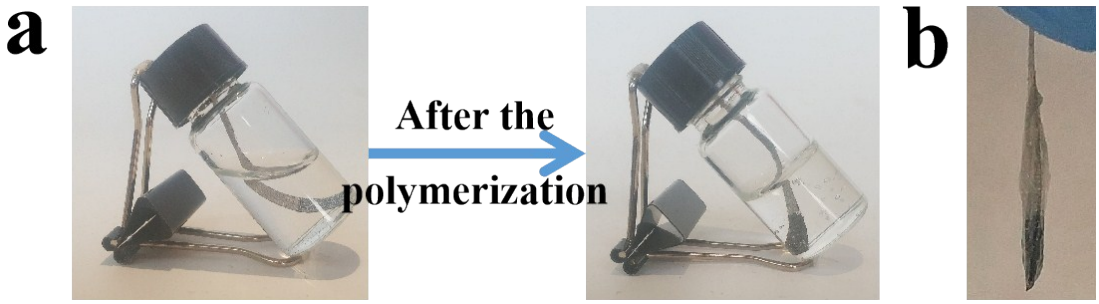

Figure S5. (a) Photographs of monomer mixture solution before and after polymerization. (b) The photograph of AC electrode with in-situ polymerized P(AA-DAC) electrolyte.

After polymerization, the electrolyte is changed into a gel state as shown in Figure S5.

When AC electrode was immersed in the monomer solution, after polymerization two sides of the AC electrode were coated with electrolytes. The solid electrolyte is tightly combined with the AC electrodes and will not flow down in the vertical state. (Figure 5b).

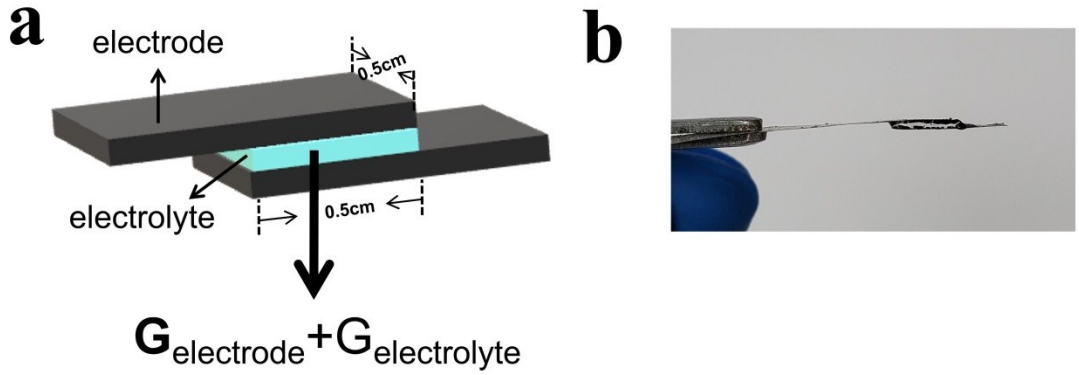

Figure S6. Schematic (a) and photograph (b) of the SC device suspended in air without any package for calculation of the sum of weight of electrode and electrolyte.

To avoid slipping or falling off, the adhesion strength between the electrode and gel electrolyte is crucial in SC device. The minimal adhesion strength necessary for the two electrodes to stick together is dependent on the kinds of electrode used. In our case, the minimal adhesion strength of electrode/electrolyte interface is the sum of the weight of AC electrode and P(AA_1-DAC_2) electrolyte as shown in Figure S6. For an area of 0.5 x 0.5 cm^2, the sum of the weight of one AC electrode (~0.0126 g) and P(AA_1-DAC_2) electrolyte (~0.0088 g) is about 0.21×10^{-3} N. The adhesion strength of electrode/electrolyte interface obtained by in-situ polymerization is about 100 N m^{-1}. The width of the electrode is 0.5 cm and the adhesion strength of electrolyte is about 0.5 N, which is much higher than the sum of the weight of electrode and electrolyte. Therefore, our electrolyte has enough adhesion strength for the two electrodes to stick together.

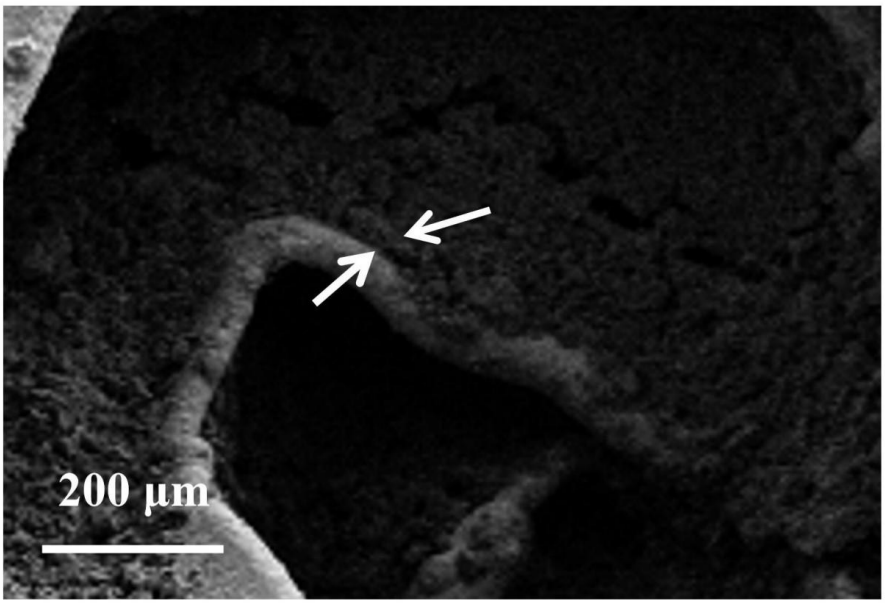

Figure S7. SEM images of pristine AC electrode (Between the two arrows is the thickness of the coated active materials).

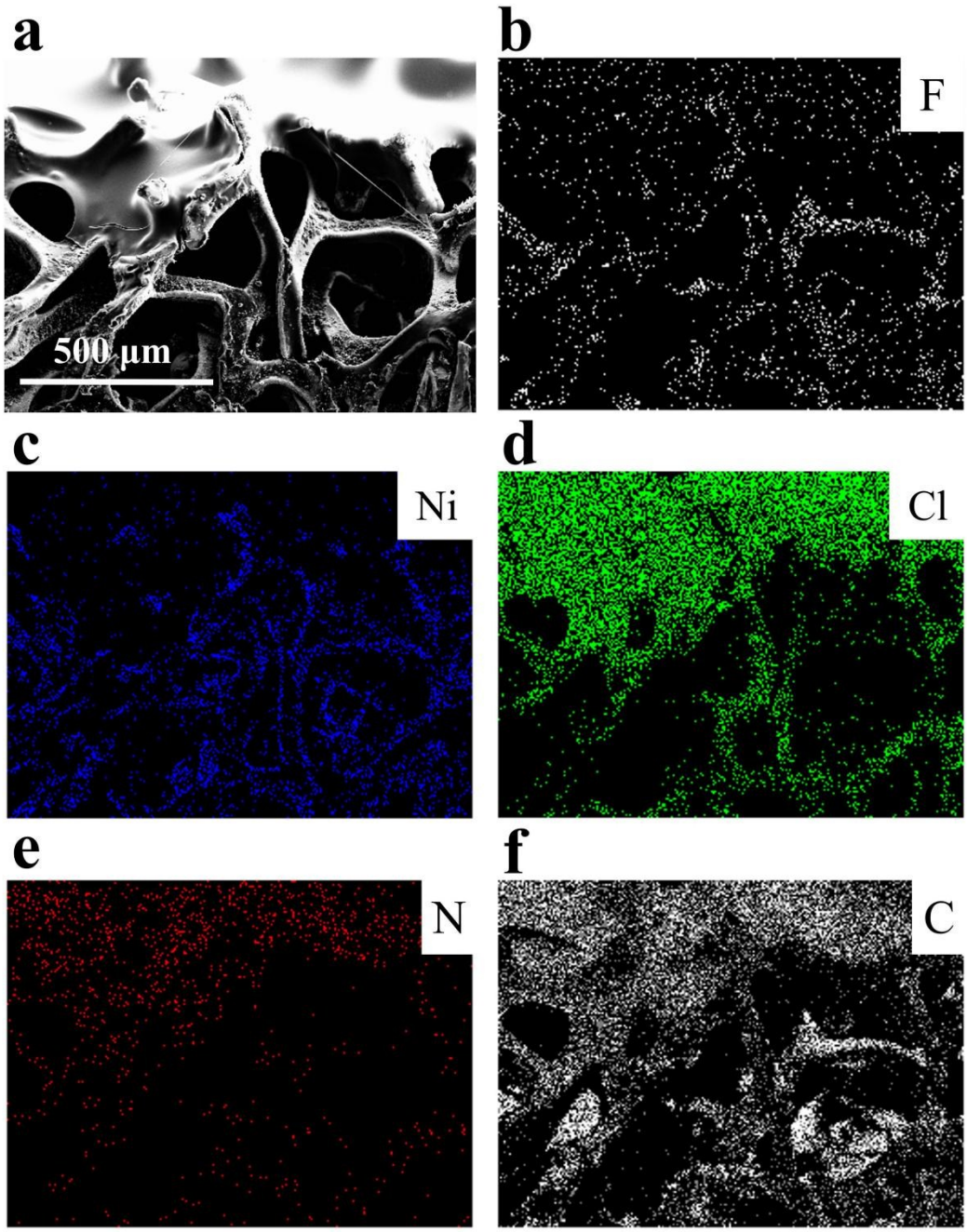

Figure S8. SEM images of AC electrode with in-situ polymerized P(AA-DAC) electrolyte (a) and corresponding elemental mapping for fluorine (b), nickel (c), chlorine (d), nitrogen (e),carbon (f), respectively.

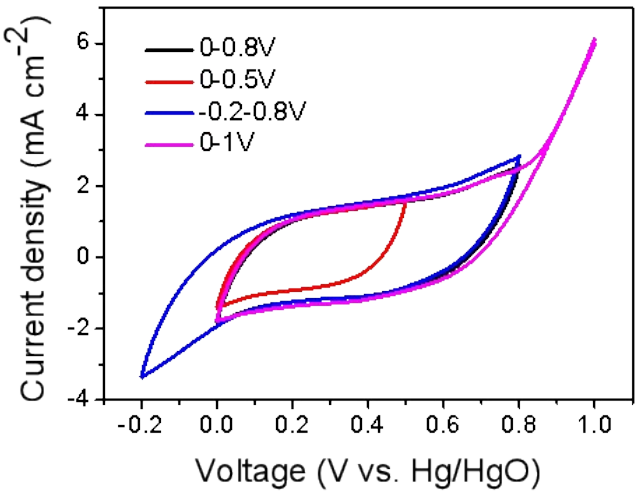

Figure S9. CV curves of AC electrode in three-electrode measurements.

The voltage window of Ni/carbon/electrolyte was first measured by three-electrode measurement method. A platinum sheet was employed as the counter electrode, and a mercury/mercury oxide electrode (Hg/HgO) as the reference electrode. The working electrode was AC electrode. The electrolyte was P(AA_1-DAC_2) hydrogel. Before measurement, the three electrodes were immersed in the electrolyte for one day to ensure the full contact between electrolyte and electrode. CV curves were tested by changing different voltage windows at the scan rate of 10 mV S^{-1}. When the voltage is less than 0 V or greater than 0.8 V, the end of the shape of the CV curve becomes deformed (Figure S9). Therefore, the voltage window of 0~0.8V is stable and appropriate.

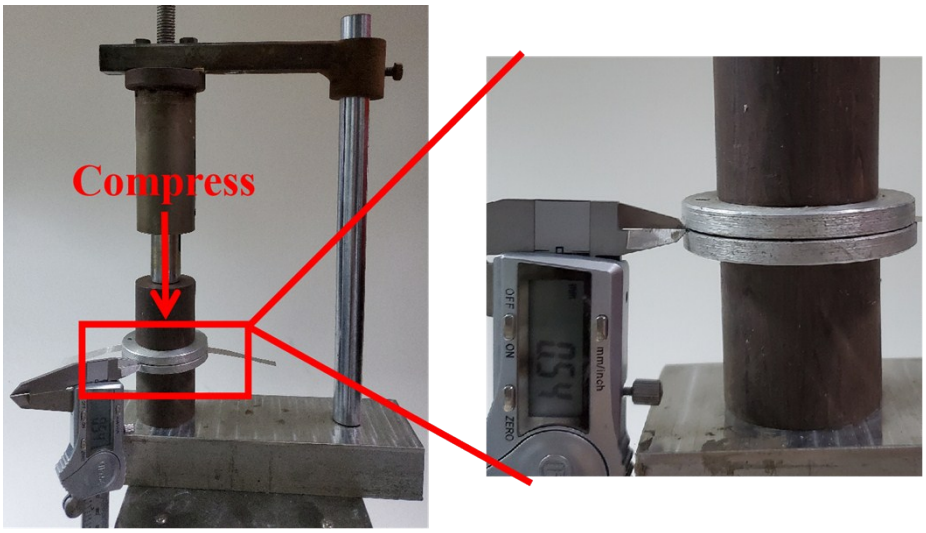

Figure S10. The thickness of the SC was controlled by a home-made compressible device.

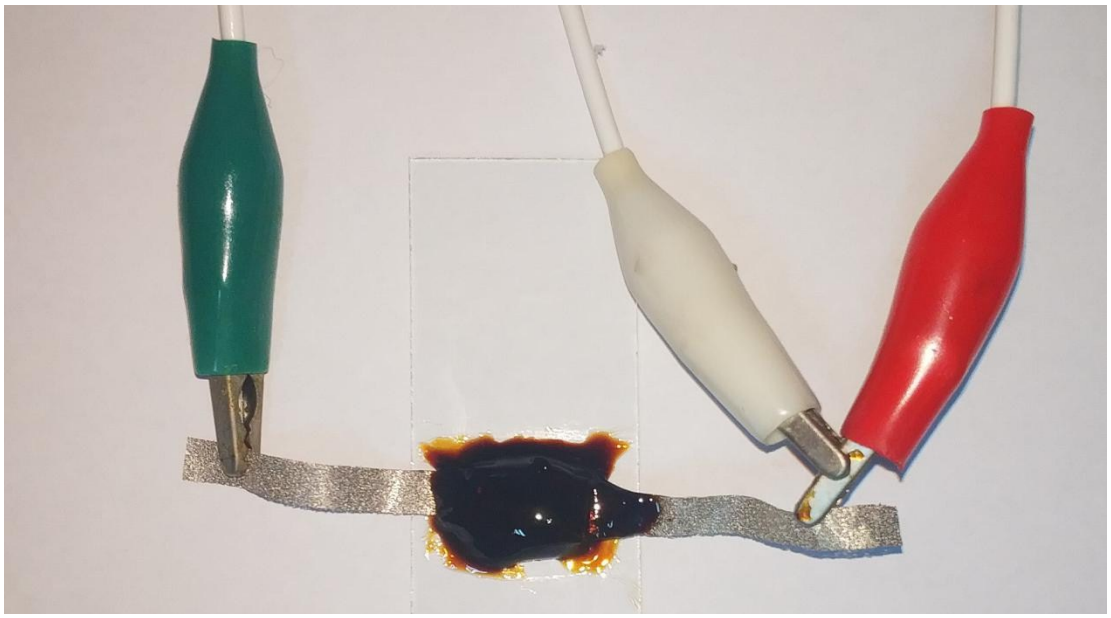

Figure S11. Solid device encapsulated by polyurethane during the electrochemical measurement.

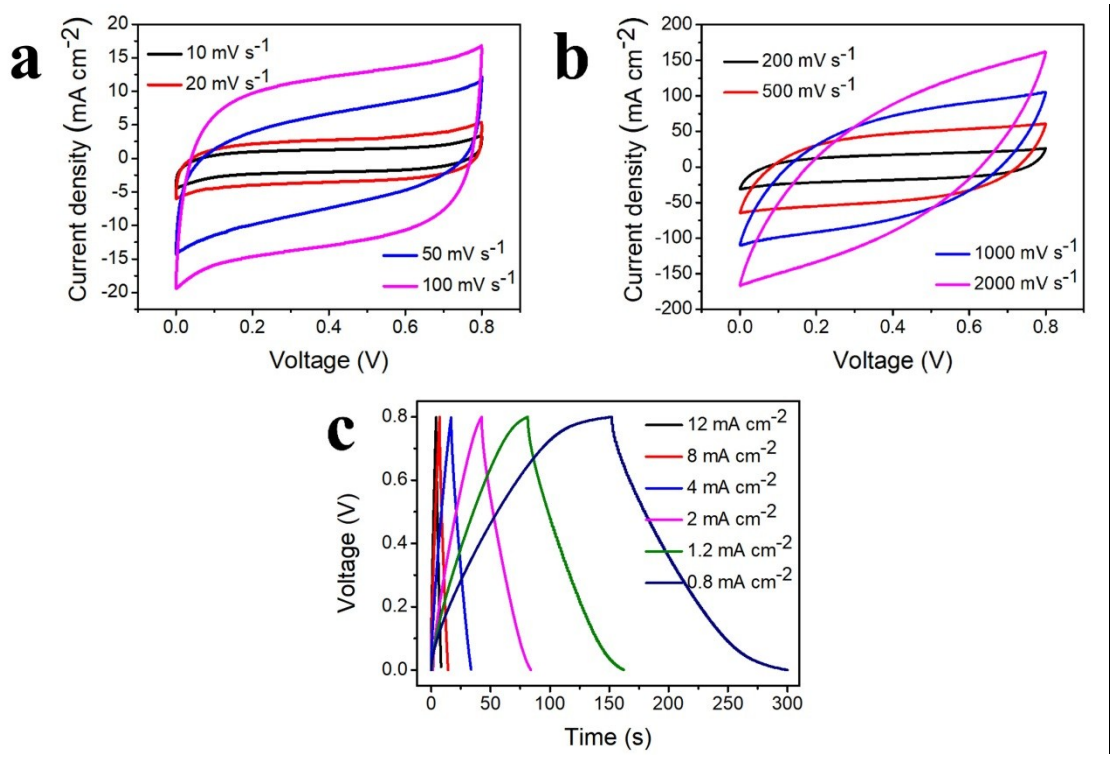

Figure S12. CV curves (a and b) and GCD curves (c) of AC electrode-based supercapacitor with P(AA_1-DAC_2) electrolyte.

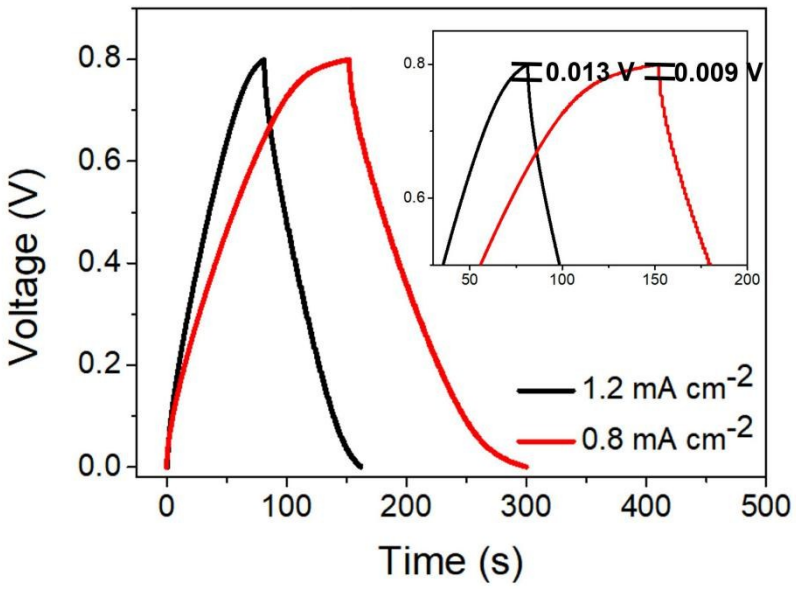

Figure S13. GCD curves of the of AC electrode-based device with P(AA_1-DAC_2) electrolyte (inset is enlarged parts of GCD curves).

The voltage drop determined from the GCD curves is about 0.009 and 0.013 V at 0.8 and 1.2 mA cm^{-2} (Figure S14). Thus, the equivalent series resistance (ESR, Ω cm^2) is 11.2 and 10.8 Ω cm^2 at 0.8 and 1.2 mA cm^{-2}, which was calculated by the following equation:

$$ESR = \frac{V_{drop}}{I_{sp}}$$

where V_{drop} is the voltage drop (V) in the discharge curve. I_{sp} is the specific current density (A cm^{-2}).

A larger charge/discharge current gave rise to a smaller ESR value, which indicates a relative slower ion-diffusion process under the low current density/scan rate[1].

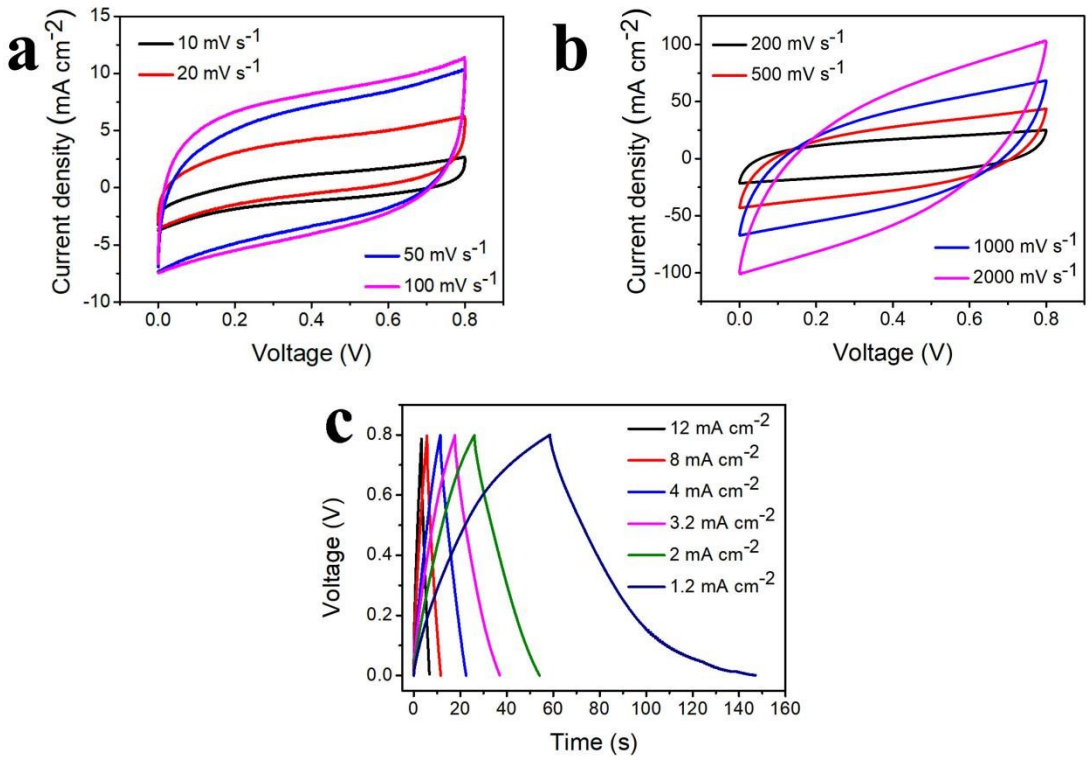

Figure S14. CV curves (a and b) and GCD curves (c) of AC electrode-based supercapacitor with PVA/LiCl electrolyte.

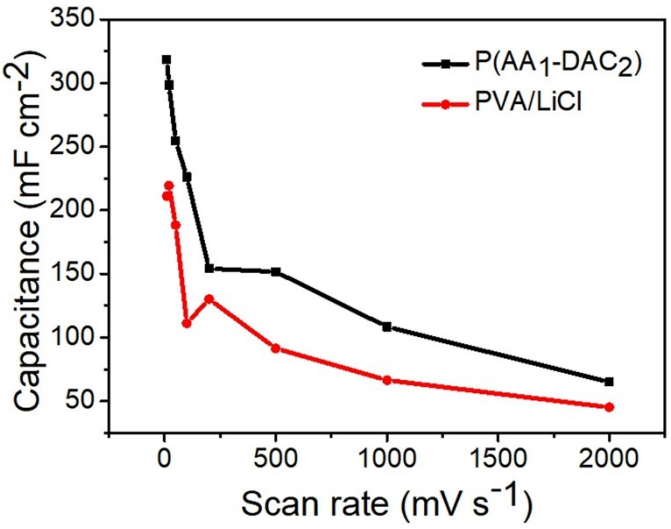

Figure S15. Specific area capacitance of AC electrode with P(AA_1-DAC_2) and PVA/LiCl electrolyte derived from CV curves.

The specific capacitance (F cm^{-2}) calculated from the CV is according to the following equation:

$$C_{sp} = \frac{1}{2 \times S_{device} \times \mathrm{v} \times \Delta V} \int_{Va}^{Vb} IdV$$

Where ΔV (V), v (V s^{-1}) and S_{device} (cm^2) are the potential window, the scan rate and the total area of two electrodes, respectively. V_b and V_a (V) are the high and low voltage limit of the CV curves.

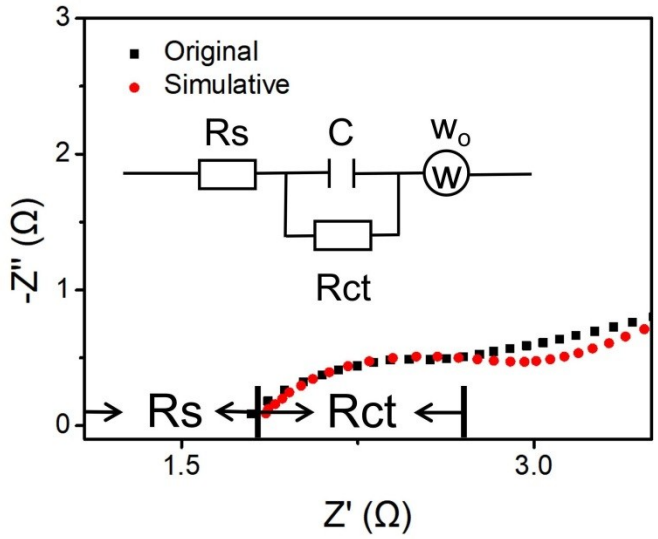

Figure S16. Electrochemical impedance curves and simulation results (inset is equivalent circuits for fitting EIS results).

In EIS measurement for electric double-layer capacitors (EDLCs), the starting point of the semicircle in the real axis of the Nyquist spectrum generated in high frequency region is solution (gel) resistance (Rs), which occurs due to ionic conductivity of the electrolyte ions. The diameter of the semicircular arc corresponds to the dynamic resistance of the charge transfer at the interface between the active electrode material and the electrolyte called Rct. The straight line in low frequency region of Nyquist plot is the double layer capacitance generated at the electrode surface. This region is governed by ability of ion migration through the pores and electrical resistivity of the electrode material[2]. In general, porous graphene aerogel with high surface area used as electrode in EDLC results in almost vertical line in low frequency region because of the highly available charge storage sites on the pore surfaces of the electrode[3 4]. In our case, active carbon was loaded on the Ni foam and used as electrode. The relative low ability of ion migration in diffusion layer and relative small amount of charge storage site of the electrode leads to the non-vertical line. In addition, we also have simulated the Nyquist plots to an equivalent circuit as shown in Figure S16. The Rs is about 1.91 Ω and Rct is about 0.79 Ω by fitting circuit.

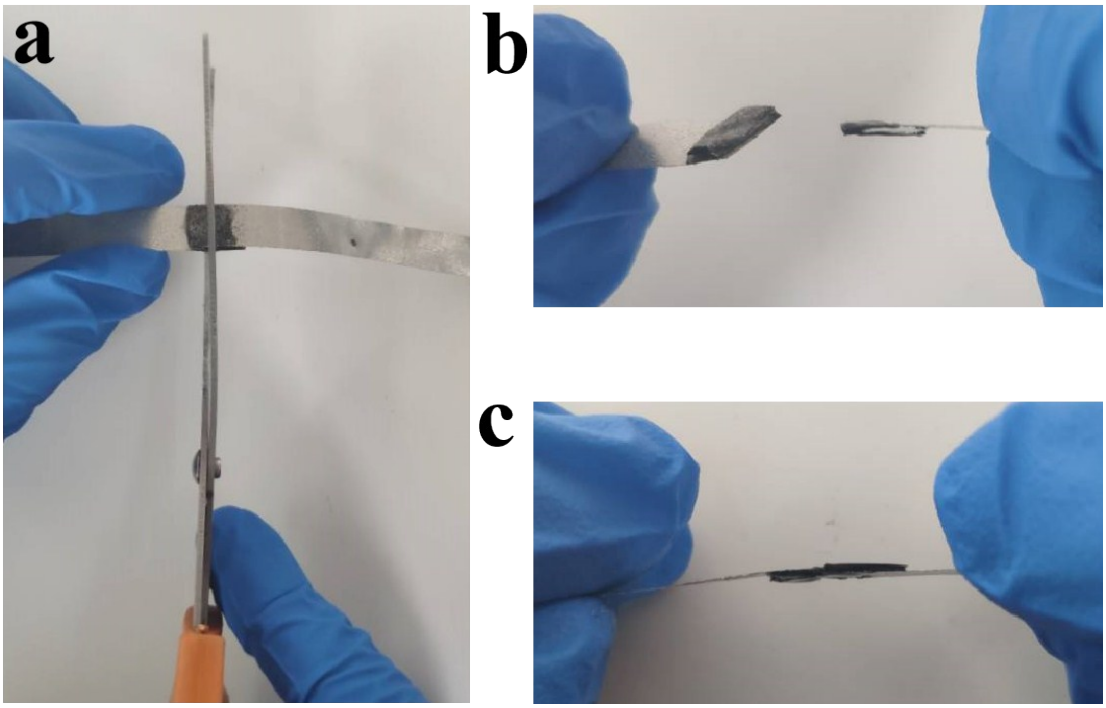

Figure S17. Photographs of the cut and self-healing test process. (a) The whole device was cut into two parts with scissor. The two parts were carefully contacted with each other (b and c).

DFT Calculation Parts：

The binding energy, E_b, between the ions and segments of AA and DAC was determined using the equations:

$\boldsymbol{E}_b1 = \boldsymbol{E}(LiCl) - \boldsymbol{E}(Cl^-) - \boldsymbol{E}(Li^+)$; $\boldsymbol{E}_b2 = \boldsymbol{E}(AA+Li^+) - \boldsymbol{E}(AA) - \boldsymbol{E}(Li^+)$;

$\boldsymbol{E}_b3 = \boldsymbol{E}(AA+DAC) - \boldsymbol{E}(AA) - \boldsymbol{E}(DAC)$; $\boldsymbol{E}_b4 = \boldsymbol{E}(AA+Cl^-) - \boldsymbol{E}(AA) - \boldsymbol{E}(Cl^-)$

where E_b1-4 are the binding energies for four cases among the two fragments in polymer and two ions, respectively. $\boldsymbol{E}$(LiCl) represents the energy of LiCl, and $\boldsymbol{E}$(AA+DAC) is the total energy of the two segments. $\boldsymbol{E}(AA+Li^+)$, $\boldsymbol{E}(AA+Cl^-)$ are the

total energies of the ions with the segment in polymer. ***E***(Cl^-), ***E***(Li^+), ***E***(AA), ***E***(DAC) are the energies of the tow ions and the two segments, respectively.

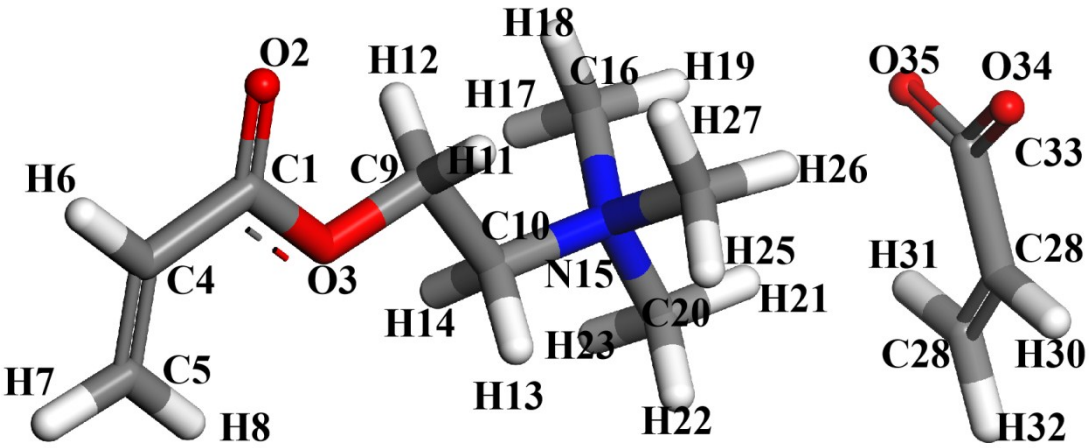

Cartesian Coordination for the optimized structures of DAC-COO
E （DAC-COO）= -493.6089x10^3 Kcal/mol

Atomic Number	Coordinates(Angstroms) X	Y	Z
6	-4.436474	0.545361	0.050818
8	-4.399638	1.756021	-0.077902
8	-3.334974	-0.220424	0.042439
6	-5.688396	-0.208918	0.229211
6	-5.758327	-1.527804	0.380095
1	-6.575739	0.410862	0.230291
1	-6.714364	-2.018752	0.50895
1	-4.875126	-2.152806	0.380863
6	-2.077982	0.464138	-0.123029
6	-1.053126	-0.653429	-0.103783
1	-1.948893	1.169429	0.695185
1	-2.08942	1.004119	-1.067229
1	-1.125664	-1.208154	0.828896
1	-1.230316	-1.330524	-0.936496
7	0.37727	-0.197912	-0.220738
6	0.606816	0.543106	-1.502331
1	0.268918	-0.080136	-2.325855

1	0.058574	1.479308	-1.480156
1	1.671271	0.741694	-1.587797
6	1.237957	-1.425509	-0.215944
1	2.273311	-1.117207	-0.313842
1	1.084757	-1.950238	0.72321
1	0.948406	-2.053327	-1.054183
6	0.772713	0.66761	0.937174
1	0.548306	0.135164	1.857479
1	1.837944	0.864661	0.864327
1	0.223745	1.602569	0.891411
6	4.947258	-0.69994	0.682147
6	5.072017	-1.769014	-0.096048
1	5.122455	-0.774103	1.749929
1	4.89688	-1.71004	-1.163675
1	5.349721	-2.734812	0.30858
6	4.555481	0.666288	0.186415
8	4.456754	1.568244	1.068212
8	4.348699	0.833201	-1.046883

Charge scheme of DAC-COO

C1	0.432232
O2	-0.456548
O3	-0.274844
C4	-0.195757
C5	-0.245463
H6	0.162407
H7	0.169718
H8	0.168836
C9	-0.077769
C10	-0.127456
H11	0.154835
H12	0.155354
H13	0.173384
H14	0.173454
N15	0.099560
C16	-0.317397
H17	0.177255
H18	0.182233
H19	0.168247
C20	-0.294627
H21	0.170290

H22	0.175347
H23	0.177475
C24	-0.319747
H25	0.177164
H26	0.173844
H27	0.180660
C28	-0.224331
C29	-0.279342
H30	0.131860
H31	0.141826
H32	0.154105
C33	0.364798
O34	-0.628544
O35	-0.623059

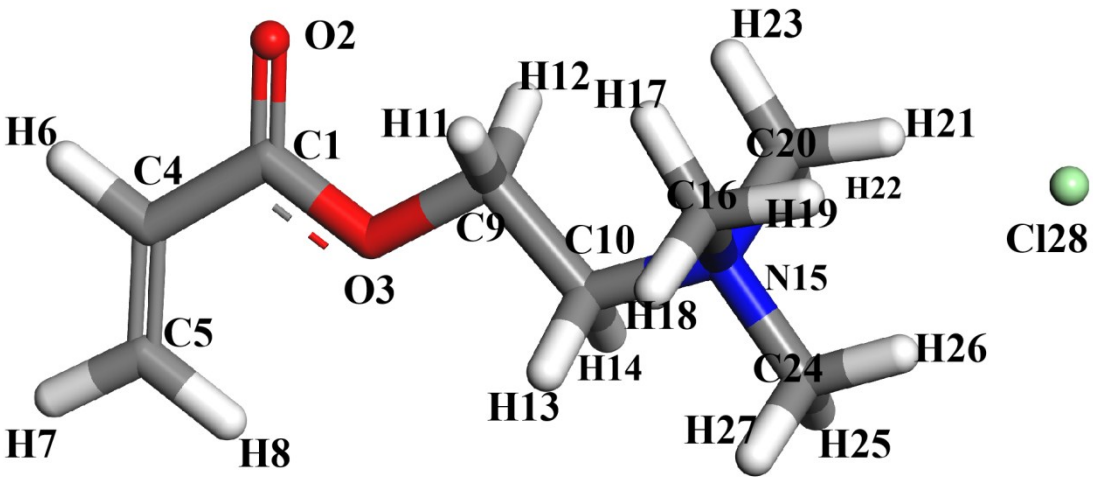

Cartesian Coordination for the optimized structures of DAC-Cl
E （DAC-Cl）= -615.0682x10^3 Kcal/mol

Atomic Number	Coordinates(Angstroms) X	Y	Z
6	-3.420686	0.660926	0.005939
8	-3.300761	1.873173	-0.003773
8	-2.371222	-0.173963	-0.002739
6	-4.726435	-0.01963	0.028196
6	-4.888207	-1.339006	0.040789
1	-5.571827	0.656301	0.03367
1	-5.879592	-1.773185	0.056984

1	-4.047361	-2.020012	0.035574
6	-1.065446	0.434732	-0.027699
6	-0.113705	-0.745388	-0.048032
1	-0.945221	1.054915	0.858078
1	-0.980879	1.055004	-0.917215
1	-0.286231	-1.376077	0.821483
1	-0.270594	-1.332333	-0.95052
7	1.343238	-0.374818	-0.024364
6	1.708878	0.335071	1.244256
1	1.203604	1.294963	1.277489
1	1.40602	-0.284868	2.083966
1	2.78757	0.480339	1.236804
6	1.711957	0.483754	-1.196428
1	2.791932	0.616727	-1.176669
1	1.398724	-0.022896	-2.105548
1	1.216184	1.445036	-1.104782
6	2.133638	-1.648355	-0.09773
1	1.882786	-2.154518	-1.026261
1	3.189522	-1.386039	-0.071015
1	1.865636	-2.266544	0.755203
17	5.186645	0.357095	0.042332

Charge scheme of DAC-CL

C1	0.432439
O2	-0.457268
O3	-0.274526
C4	-0.196336
C5	-0.245228
H6	0.162126
H7	0.169632
H8	0.168804
C9	-0.076767
C10	-0.126763
H11	0.151874
H12	0.154501
H13	0.171327
H14	0.171103
N15	0.100608
C16	-0.309048
H17	0.176346
H18	0.172098

H19	0.144151
C20	-0.311628
H21	0.145334
H22	0.172678
H23	0.177884
C24	-0.286517
H25	0.170874
H26	0.145107
H27	0.170483
Cl28	-0.873288

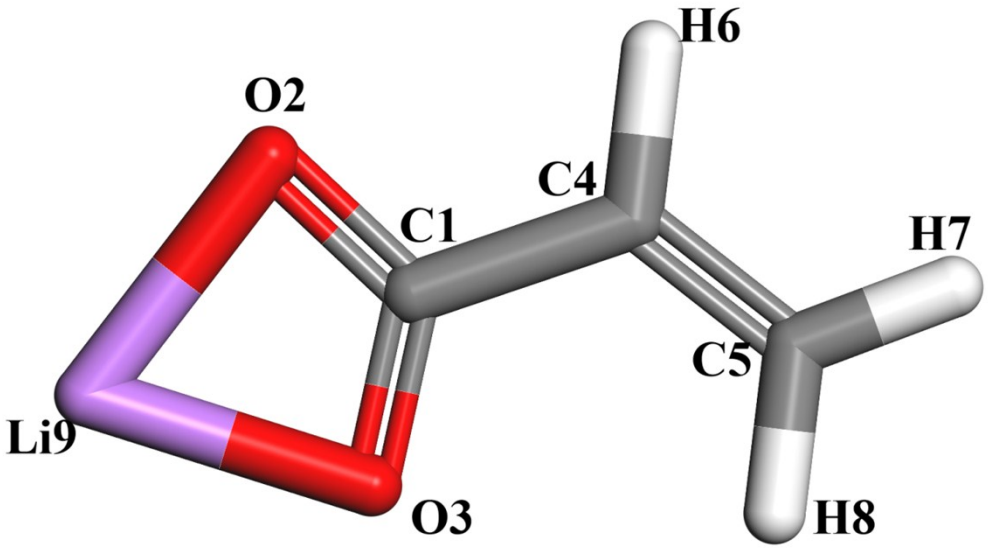

Cartesian Coordination for the optimized structures of COO-Li
E （COO-Li）= -172.1364x10^3 Kcal/mol

Atomic Number	Coordinates(Angstroms) X	Y	Z
6	-0.36495	0.099539	0.000023
8	-1.292099	0.971371	0.000043
8	-0.634452	-1.141448	-0.00004
6	1.043028	0.575173	-0.000032
6	2.088254	-0.244788	0.000036
1	1.171437	1.650887	-0.000212
1	3.102111	0.135326	-0.000073
1	1.95962	-1.320316	0.000174
3	-2.472918	-0.561608	-0.000024

Charge scheme of COO-Li

C1	0.481050
O2	-0.668392
O3	-0.663939
C4	-0.181273
C5	-0.263666
H6	0.146371
H7	0.163140
H8	0.152745
Li9	0.833964

References

1. Li, J.; Wang, N.; Tian, J.; Qian, W.; Chu, W., Cross-Coupled Macro-Mesoporous Carbon Network toward Record High Energy-Power Density Supercapacitor at 4 V. *Advanced Functional Materials* **2018,** *28* (51), 1806153.
2. Bhattacharjya, D.; Yu, J.-S., Activated carbon made from cow dung as electrode material for electrochemical double layer capacitor. *Journal of Power Sources* **2014,** *262*, 224-231.
3. Du, Y.; Liu, L.; Xiang, Y.; Zhang, Q., Enhanced electrochemical capacitance and oil-absorbability of N-doped graphene aerogel by using amino-functionalized silica as template and doping agent. *Journal of Power Sources* **2018,** *379*, 240-248.
4. Li, T.; Ding, Y.; Liu, L.; Liu, J.; Fang, W.; Xiang, Y.; Li, T., Facile fabrication of multifunctional perfluoroalkyl functionalized graphene hydrogel via a synchronous reduction and grafting strategy. *Journal of Materials Chemistry A* **2015,** *3* (43), 21744-21753.